Voltammetry using multiple cycles: Porous electrodes

Henry T. H. Chan, Enno Kätelhön, Richard G. Compton

Department of Chemistry, Physical and Theoretical Chemistry Laboratory, Oxford University, South Parks Road, Oxford, OX1 3QZ, United Kingdom

Abstract

Simulations are reported for the cyclic voltammetry of both electrochemically reversible and irreversible one-electron processes at porous electrodes where the potential cycle is applied for multiple cycles. It is shown that an 'ultimate state' is approached asymptotically and that the long time voltammogram can be very different in terms of the peak height from those recorded in the first scan though peak-to-peak potential separations are conserved. The implications for the experimental study of porous electrodes are considered.

Keywords

Multiple-cycle voltammetry, porous electrodes, ultimate state.

1 Introduction

Cyclic voltammetry[1;2] is ubiquitously applied for the study of electrochemical processes and is familiar to all electrochemists as, at least, an initial starting point for their investigations. Ensuring that mass transport to and from the electrode occur exclusively via diffusion, the method involves the application of a triangular potential waveform to a working electrode as part of a conventional three electrode system[3;4].Current (I) is then measured as a function of the applied potential (E). The resulting voltammogram is characterised by the magnitude of the peak currents (I_p) and the peak-to-peak potential differences (ΔE_{pp}), see Figure 1. The expected behaviour for both fast ('reversible') and slow ('irreversible') electrode transfer kinetics is well known and described in terms of the peak currents by the Randles-Ševčík equations for a simple one electron process, $A + e \rightarrow B$:

$$I_p^{RS} = 0.446FAc_i^*\sqrt{\frac{FD_iv}{R_uT}} \quad \text{(reversible)} \tag{1}$$

$$I_p^{RS} = 0.496\sqrt{\alpha}FAc_i^*\sqrt{\frac{FD_iv}{R_uT}} \quad \text{(irreversible)} \tag{2}$$

where F is Faraday constant, A is the surface area of the electrode, c_i^* is the bulk concentration of species i, D_i is the diffusion constant of species i, v is the potential scan rate, R_u the universal gas constant, T is the temperature, and α[5;6] is the transfer coefficient.[3;4] The peak-to-peak separation is given by:[4]

$$\Delta E_{pp} = 2.218\frac{R_uT}{F} \quad \text{(reversible)} \tag{3}$$

$$\Delta E_{pp} = \frac{2R_uT}{F}ln\ v + const. \quad \text{with} \quad \alpha = \frac{1}{2} \quad \text{(irreversible)} \tag{4}$$

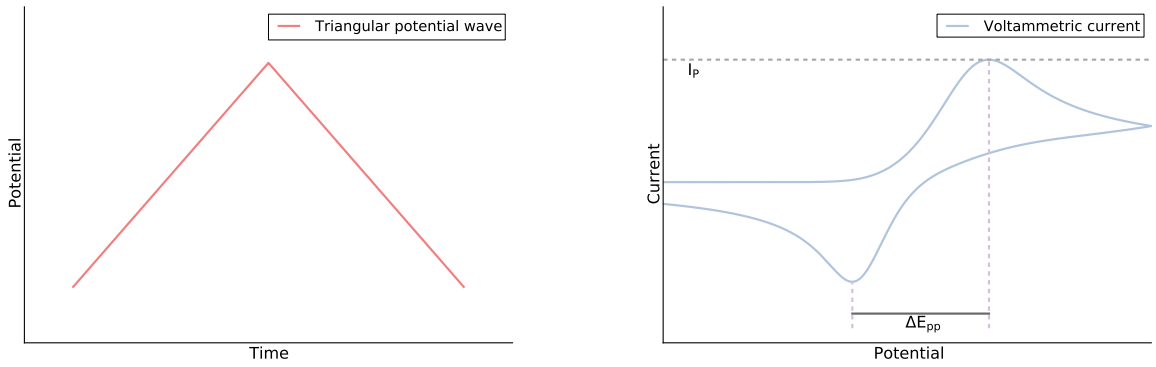

Figure 1: Illustration of the triangular potential wave applied in cyclic voltammetry and the most significant quantities that can be extracted from a voltammogram.

The full voltammogram is readily computed via numerical simulation of the coupled transport (Fick's law) and electron transfer (Butler-Volmer) equations via either commercial products (DIGISIM, Comsol, etc.) or as self-written code[7], as well as being documented in the various voltammetry textbooks[3;4].

The theoretical results for I_p and ΔE_{pp} given above relate to the *first* voltammetric scan, and it is important that voltammetric data analysed are measured accordingly. The reason for this is that second and subsequent cycles retain a 'memory' of the earlier scan(s) since, unless the number of potential cycles scanned is infinite, there is, in the reverse scan, incomplete reversal of the charges induced on the forward scan. Accordingly, if experimentalists choose to apply multiple potential cycles to systems (often in order for "it to stabilise"), then any quantitative analysis must reflect the changes induced by any prior scans. In this context, it is interesting to question the changes in voltammetric signals which accompany a very large number of potential scans. Insightful work by Oldham[8;9] has shown that for the case of semi-infinite diffusion to a macrodisc electrode, the voltammogram, under some circumstances, converges to a final unchanging form given the label of an 'ultimate limit' by Oldham.

The practice of multiple potential cycles is probably most often applied in the study of electrodes modified with porous layers.[10;11] In this paper, we use numerical simulation to investigate multiple-cycle voltammetry at porous electrodes noting that from previous simulations of the single cycle case the voltammetric response will contain components reflecting both semi-infinite diffusion and thin-layer type behaviour.[4;12;13] We explore whether 'ultimate states' exist for voltammetry at porous electrodes and show the extent to which multiple cycles can deviate from first cycle voltammetry.

2 Theoretical model

Our study is based on a model[12] discussed by Ban *et al.*, which was formerly employed in the investigation of staircase voltammetry at porous surfaces and considered a large number of equally-sized cylindrical electrodes that were mounted on an insulating surface in an upright orientation. The modelled geometry hence approximates the structure of porous electrode formed from individual fibres, which for instance may resemble an electrode modified with carbon nanotubes (so-called 'nanotube forests'). This section briefly outlines our calculations, while more detailed information can be found in the original study.

The presented modelling approach is based on the diffusion domain approximation[14–18], which under certain circumstances enables the conversion of a complex three-dimensional electrode structure to a significantly simpler two-dimensional geometry. Making use of the symmetry of the surrounding space experienced by the cylindrical

electrodes, one can identify the average area of the supporting surface that is allocated to each cylinder if considered as a Voronoi grid, determine its average value, and define an equally-sized bottom area of a virtual three-dimensional simulation space featuring the shape of an upright cylinder whose symmetry axis aligns with the symmetry axis of the electrode. Since all electrodes are assumed to be equal, all characteristics of the systems must then be symmetric with respect to the girthed area of the simulated space, i.e. its surface area minus the top- and bottom boundaries. Due to the models symmetry with respect to the cylinders' longitudinal axis, the geometry can further be simplified to a two-dimensional space solely considering the longitudinal and the axial dimension as depicted in Figure 2. Please note that the figure illustrates the geometry alongside the corresponding boundaries, which are discussed in more detail below.

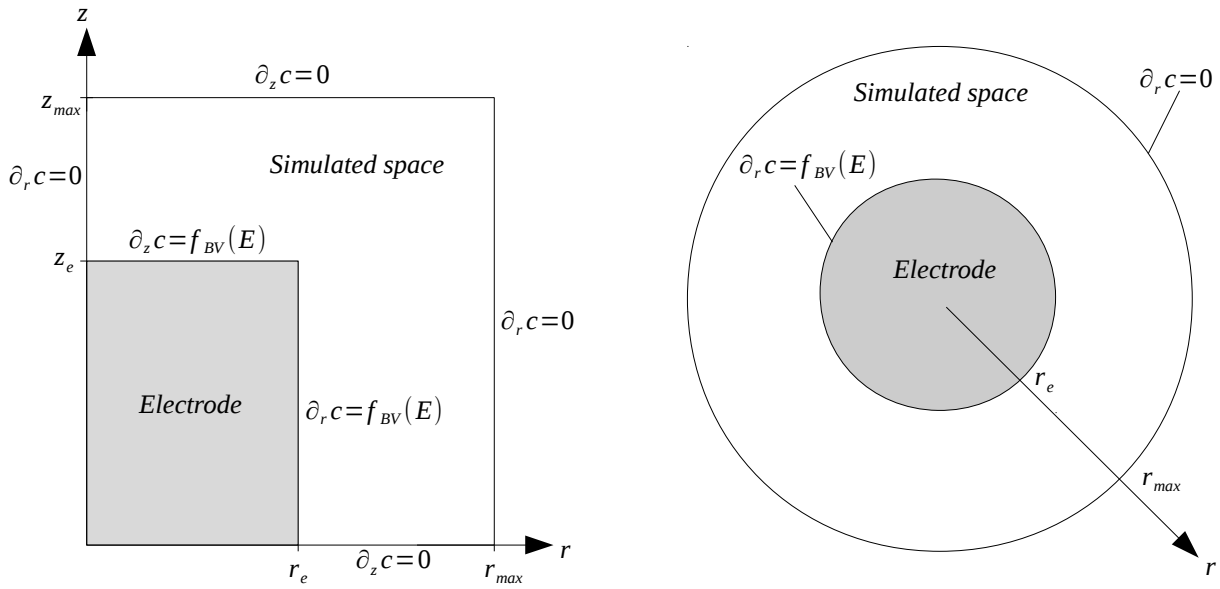

Figure 2: Illustration of simulated geometry including the boundary conditions that are considered when solving diffusion equation. It is noted that dimensions are not ploted to scale. [figure was amended]

Due to the small electrode size, the relatively short time scale on which an experiment is performed, and the assumed presence of adequate supporting electrolyte, we can neglect any mass transport effects other than diffusion to good approximation[19] and describe all mass transport via diffusion equation*:

$$\partial_t c_i(\vec{r},t) = D_i \Delta c_i(\vec{r},t) \tag{5}$$

which is solved subject to appropriate boundary conditions and where $c_i(\vec{r},t)$ is the concentration of the diffusing species i at the position $\vec{r}$ and the time t, D_i the corresponding diffusion coefficient, and Δ the Laplace operator, $\Delta = \vec{\nabla}^2$, which in the case of the here-considered cylindrical coordinates and rotational symmetry with respect to the z-axis is given by $\Delta = \partial_r^2 + r^{-1}\partial_r + \partial_z^2$.

The boundary conditions are partly determined by the electrode kinetics, the initial concentration, and through additional equations arising from the diffusion field approximation. We herein consider two chemically

*In this context we note that in non-adsorbing porous materials, which confine the space available for the analyte mass transport to dimensions of the order of only few molecule volumes, the mass transport may rather be determined by surface interactions and mechanisms different from Equation (5) may be prevalent. It is further noted that in the cases of very slow and fast scan rates, effects arising from thermal convection in conjunction with density fluctuations of the analyte and buoyancy forces, the electrode impedance, and Nernst-Planck equation may become apparent. Under standard experiential conditions all of these will however not contribute significantly to the observed currents.

stable species A and B that feature equal diffusion coefficients, $D_A = D_B$, and participate in the following heterogeneous reaction at the electrode surface:

$$A + e \rightarrow B \tag{6}$$

Since both feature equal diffusion coefficients, it is sufficient to model solely the diffusion of one species as conservation of mass generally yields the following condition at all positions $\vec{r}$ in space:

$$\sum_{i=A,B} c_i^* - c_i(\vec{r}, t) = 0 \tag{7}$$

if initially the system is in equilibrium and the concentrations of A and B are homogeneous. We further assume that the reaction can be approximated through Butler-Volmer kinetics, which leads to the following boundary conditions at the electrode surface:

$$\begin{aligned} D\ \partial_r c_A(\vec{r}, t)\Big|_{r=r_e,\ z\leq z_e} =& k_0\ exp\left(\frac{-\alpha F(E - E_f^0)}{RT}\right) c_A(\vec{r}, t) \\ &- k_0\ exp\left(\frac{(1-\alpha) F(E - E_f^0)}{RT}\right) (c_A^* - c_A(\vec{r}, t)) \end{aligned} \tag{8}$$

$$\begin{aligned} D\ \partial_z c_A(\vec{r}, t)\Big|_{r\leq r_e,\ z=z_e} =& k_0\ exp\left(\frac{-\alpha F(E - E_f^0)}{RT}\right) c_A(\vec{r}, t) \\ &- k_0\ exp\left(\frac{(1-\alpha) F(E - E_f^0)}{RT}\right) (c_A^* - c_A(\vec{r}, t)) \end{aligned} \tag{9}$$

where we set $D = D_A = D_B$ and $c_B^* = 0$. The boundary at the supporting surface as well as in the bulk are further set to 'no flux' boundaries, i.e. the concentration gradient vanishes and according to Fick's law for the flux $j = \partial_{r,z} c(\vec{r})$, no material is generated or removed.

$$\partial_z c(\vec{r}, t)\Big|_{r>r_e,\ z=0} = 0 \tag{10}$$

$$\partial_z c(\vec{r}, t)\Big|_{z=z_{max}} = 0 \tag{11}$$

In addition, we implement the boundary conditions that arise from the symmetry of the geometry and the diffusion domain approximation. The systems geometry with regard to the longitudinal axis necessarily implies that any flux of material must vanish at $r = 0$, i.e.:

$$\partial_r c(\vec{r}, t)\Big|_{r=0,\ z>z_e,} = 0 \tag{12}$$

As discussed above, the diffusion domain approximation further exploits the symmetry of the concentration profile with respect to the boundary to neighbouring diffusion domains, which yields the condition:

$$\partial_r c(\vec{r}, t)\Big|_{r=r_{max}} = 0 \tag{13}$$

For clarity and more universal applicability of our results, we transform the above equations to dimensionless

coordinates according to the identities provided in Table 1 and present all results in dimensionless quantities.

Parameter	Dimensionless equivalent
Concentration	$C_j = \frac{c_j}{c_A^*}$
Radial distances	$R = \frac{r}{r_e}$
	$R_e = \frac{r_e}{r_e} = 1$
	$R_{max} = \frac{r_{max}}{r_e}$
Axial distances	$Z = \frac{z}{r_e}$
	$Z_e = \frac{z_e}{r_e}$
Time	$\tau = \frac{D_A t}{r_e^2}$
Rate constant	$K_0 = \frac{r_e k_0}{D_A}$
Scan rate	$\sigma = \frac{r_e^2 F v}{D_A R_u T}$
Potential	$\theta = \frac{F}{R_u T}(E - E_f^0)$
Current	$J = \frac{I}{2\pi F r_e D_A c_A^*}$

Table 1: Conversions from dimensional to dimensionless parameters.[7;12]

3 Computational methods

The above mass transport equations are solved numerically via a Finite Difference approach. To this end, we discretise space in an expanding grid:

$$R_i = \begin{cases} R_{i-1} + h\omega^{(i-1)} & \text{for } 0 < R \leq \frac{1}{2}R_e \\ R_{i-1} + h\omega^{(i_e - i)} & \text{for } \frac{1}{2}R_e < R < R_e \\ R_e + h\omega^{(i - i_e - 1)} & \text{for } R_e \leq R \leq R_{max} \end{cases} \tag{14}$$

and:

$$Z_j = \begin{cases} Z_{j-1} + h\omega^{(j-1)} & \text{for } 0 < Z \leq \frac{1}{2}Ze \\ Z_{j-1} + h\omega^{(j_e - j)} & \text{for } \frac{1}{2}Ze < Z < Z_e \\ Z_e + h\omega^{(j - j_e - 1)} & \text{for } Z_e \leq Z \leq Z_{max} \end{cases} \tag{15}$$

where $R_0 = 0$, $Z_0 = 0$, i and j are the indices of the grid points in the dimensions R and Z respectively, h is the size of the first spatial increment, ω is the space expansion coefficient with $\omega > 1$, i_e and j_e signify the indices that correspond to the positions of the spatial extent R_e and Z_e of the electrode, and $Z_{max} = Z_e + 6\sqrt{T_{max}}$ where T_{max} is the period of one triangular potential wave. It is herein noted that the two boundaries of central interest are the electrode boundaries and their corner, where the employed grid features the highest density of points.

As solving the present problem via the Finite Difference method involves a significant computational work-

load, we employ the alternating direction implicit [...] (ADI) method † to approximate and simplify our calculations. In short, the ADI approach regards each time step ΔT as two half time-steps that either determine the concentration profile in R dimension implicitly while calculating the Z dimension explicitly, or *vice versa*, and are solved separately via the Thomas Algorithm. Each concentration profile is then calculated on the basis of the concentration profile simulated for the previous half time step, which leads to a higher accuracy in R dimension after an implicit R half time-step, while more accurate results in Z are obtained after the corresponding time-step in Z. At each half time step, the dimensionless flux at the surface of the electrode is hence alternately calculated as:

$$\begin{aligned} J_Z &= \int_0^{Z_e} dZ\ J_i \quad \text{with} \quad J_i = -\partial_R C\Big|_{R=R_e,\ Z\leq Z_e} \\ J_R &= \int_0^{R_e} RdR\ J_j \quad \text{with} \quad J_j = -\partial_Z C\Big|_{R\leq R_e,\ Z=Z_e} \end{aligned} \tag{16}$$

where J_i and J_j are the fluxes at positions i and j on the electrode surfaces, respectively, and J_R and J_Z the corresponding flux densities in R and Z direction. The total flux to the electrode for a full time step is then given by:

$$J = J_R + J_Z \tag{17}$$

[...].

Table 2 depicts the electrochemical parameters used in our simulations, while Table 3 presents the additional parameters required for the numerical solver. The scan rate σ varies between different simulations and is provided alongside the respective plots. We further note that all electrode kinetics are modelled through the above simulation software which implements Butler-Volmer type boundary conditions. In the fully-reversible case, we herein set the electrochemical rate constant K_0 to a an arbitrary high value of 10^{10}, which yields true reversible behaviour at all considered scan rates as it is demonstrated below.

Parameter	Value
R_e	1
Z_e	50
R_{max}	1.1
K_0 (irreversible)	10^{-7}
K_0 (reversible)	10^{10}
α	0.5

Table 2: Dimensionless parameters used in all simulations.

Parameter	Value
h	10^{-5}
ω	1.06
$\Delta\theta = \lvert\sigma \cdot \Delta T\rvert$	0.01

Table 3: Parameters of no physical significance that required for numerical simulations.

The simulation is written in $C++$ and makes use of the application programming interface $OpenMP$ for

†It is noted that the ADI method is a standard tool and of no particular interest in the context of this work. We would nonetheless like to direct the interested reader to standard textbooks on numerical methods: A detailed description with a focus on electrochemical problems is for instance provided in the book [7], Chapter 9, where a full derivation, discretised equations in cylindrical coordinates, and example code can be found.

parallel computing. Further data processing and -visualisation is done in *Python* using the packages *NumPy* and *matplotlib*. The simulation parameters shown in Table 3 are chosen in a way that the height of the first peak and the peak-to-peak separation in the first cycle do not deviate more than 1% from the theoretical result if applicable.

To ensure the functionality of the software, we ran several tests[20] on the programme. For the reversible system, we verified the peak heights and peak separatons against the theoretical values at the Randles-Ševčík limit[4;20]. As for the irreversible system, we compared the potentials of the peak currents, as well as peak heights to the theoretical results[4;20] where applicable.

4 Results and discussion

In the following, we first address the case of fully-reversible electrode kinetics in multiple subsequent scans when the triangular potential wave is either centred at the reaction's formal potential (below referred to 'symmetrical') or at a different position ('asymmetrical'), before we present a similar investigation for the case of irreversible kinetics.[‡]

4.1 Reversible electrode kinetics

In spite of the complex geometry of the considered electrode, analytical results exist for various limiting cases and can be used as references in the context of this work. On one hand and in the case of an infinitely fast scan rate, the diffusion field of the electrode is compressed to an infinitesimally thin layer and the voltammetric response of the electrode resembles the response of a one-dimensional system adjacent and orthogonal to the electrochemically active surfaces, allowing a direct comparison of the first scan to the corresponding theory: The peak-to-peak separation adopts the theoretical value[4] of 2.218 for an ideally-reversible reaction as obtained from Equation (3) and the height of the peak formed in the first scan follows Randles-Ševčík equation (1) where the parameter A is the surface area of the electrode, $A = \pi r_e(r_e + 2z_e)$. On the other hand, infinitely slow scan rates equally resemble the response of a one-dimensional system as the current response arising from electroactive material initially located in between different electrodes, which is located at the right of the electrode in the diffusion domain approximation as shown in Figure 2, is far exceeded by the contribution of material that is initially located above the electrode and can be neglected. We then observe one-dimensional diffusion with respect to the longitudinal axis of the diffusion domain rather than the normal vector of the electrode surface: While the same peak-to-peak separation as in the case of an infinitely fast scan rate is found, the Randles-Ševčík equation is calculated with respect to the area of the supporting surface in the diffusion domain, $A = \pi r_{max}^2$. Both of the limiting cases can further be compared with results[8] obtained by Oldham. He shows that reversible 'ultimate cyclic voltammograms' generally exhibit a peak-to-peak separation similar to the peak-to-peak separation of the initial scan and that in case of equal diffusion coefficients and a potential scan wave symmetrical with respect to the half-wave potential, the heights I_p^O of the oxidation and reduction peaks are equal and adopt a value of:

$$I_p^O = 0.3708FAc_i^* \sqrt{\frac{FD_i v}{R_u T}} \tag{18}$$

Voltammograms simulated for a symmetrical scan window with respect to the formal potential are shown in Figure 3, which presents data for three different scan rates covering a range of eleven orders of magnitude. A closer investigation of the data reveals that various aspects of the above theory are reflected. In the slow

[‡]The terms electrochemically 'reversible' and 'irreversible' are herein meant in a strict textbook-type sense, i.e. reversible kinetics reactions approximate Nernstian behaviour and irreversible kinetics lead to fully separated forward- and backward peaks.

and in the fast case, the height of the first peaks match the values predicted by Randles-Ševčík equation and hence confirm that the electrode is operated in the linear-diffusion limit, while the heights of subsequent peaks asymptotically approach the values predicted by Oldham, i.e. local minima and maxima converge to $|min(I(t))| = |max(I(t))| = I_p^O$. In contrast to these voltammograms and at the intermediate scan rate, we observe thin-layer diffusion behaviour [12] leading to an entirely different voltammetric shape. Voltammograms are almost symmetrical with respect to the current- and the potential axis and hardly change with the progressing scan number. This observation can be understood as follows: The scan rate is chosen in a way that thin-layer diffusion dominates the voltammogram, i.e. the contribution of electroactive material that is initially located in between cylinders dominates the current response, while only a comparably small amount of material reaches the electrode from the solution above the electrode. On the time scale of the measurement, a thermodynamic equilibrium is then quickly established in between different cylindrical electrodes suppressing any memory effects during a single voltammogram as well as during the experiment comprising a total of 50 scans.

The prevalence of thin layer effects is dependent on the electrode geometry, where the electrode height Z_e and the distance between two adjacent cylinders $2R_{max}$ are of particular relevance. With an increasing electrode height, thin layer effects will become more apparent as the amount of electroactive material that reaches the electrode from within the pore increases in comparison to the amount that diffuses to the electrode from the bulk above. At a given scan rate an increase in the pore width on the one hand leads to more electroactive material being available for thin layer diffusion but on the other reduces the thin-layer character of the voltammetric response as the space available for diffusion increases.

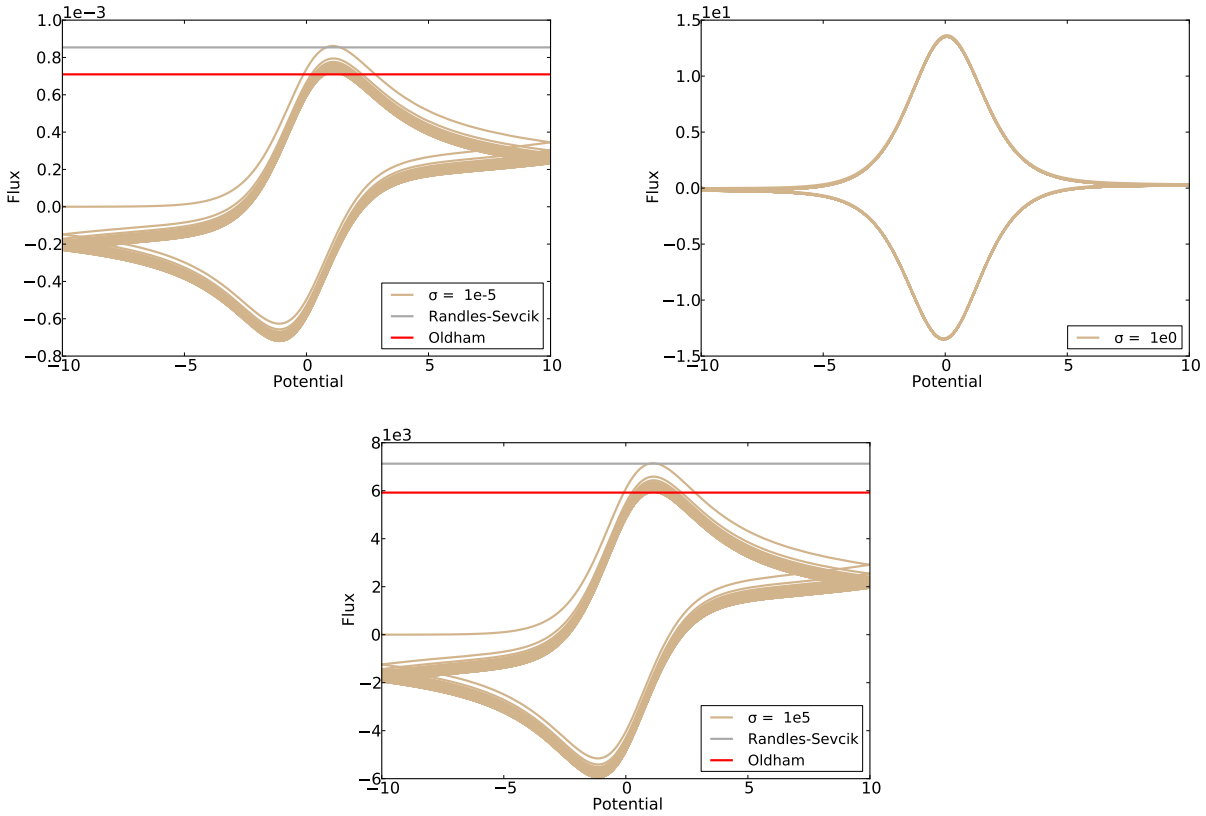

Figure 3: Fully-reversible and symmetrical voltammograms modelled for scan rates of $\sigma = 10^{-5}$, 1, and 10^5. Where applicable theoretical models are shown alongside the simulated data: Figure a) and c) plot the theoretical peak heights (1) and (18) for one-dimensional systems evaluated with respect to the corresponding surface area A.

The above findings are further supported by Figure 4, which presents the observed heights of the positive peaks as a function of the scan rate and for selected scan numbers. The plot clearly shows that peaks heights at slow and fast scan rates exhibit significant variations with the scan repetition, while peak heights in the thin-layer diffusion regime are hardly affected. In addition, we find the square-root dependency of the peak height on the scan rate as predicted by Randles-Ševčík equation (1) as well as the linear dependency in the thin layer regime, $max|I_p| \propto v$, which was previously reported[12] by Ban *et al.*.

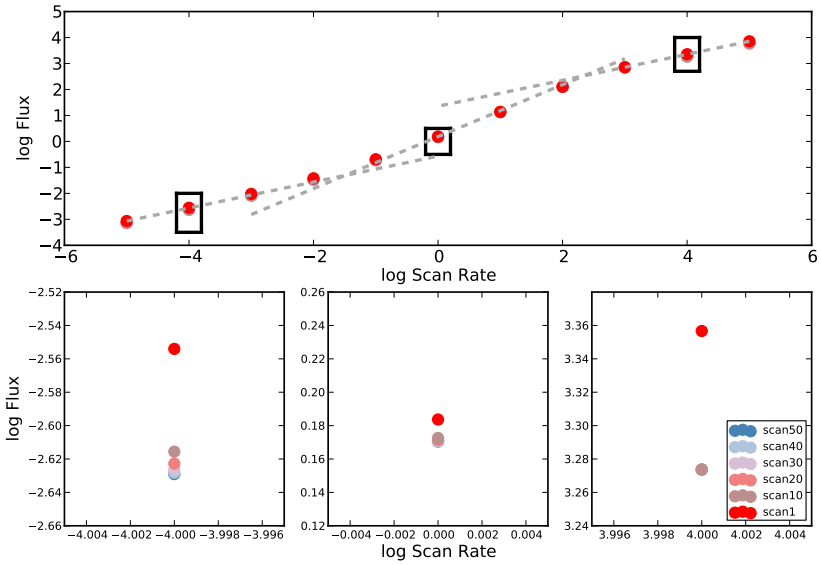

Figure 4: Maximum currents observed in reversible and symmetrical voltammograms at different scan repetitions and for various scan rates. Data is plotted alongside dashed lines featuring slopes of 0.5 and 1 in the log-log plot. The three smaller plots at the bottom of the figure amplify various regions for clarity, where it is however not that the corresponding rectangles in the main plot solely indicate the respective region and are not plotted to scale. We further note that here and in the below Figures the logarithm is calculated with respect to the base 10.

Figure 5 describes the evolution of the peak-to-peak separation as a function of the scan repetition, while a wide range of scan rates is considered. Herein, we further illustrate the shift of ΔE_{pp} from the theoretical value of 2.218 that Equation (3) predicts for a one-dimensional reversible system to a value of zero as expected for the case of thin-layer diffusion and *vice versa*. In addition, we find that much in contrast to the peak height, ΔE_{pp} is independent of the scan number for all considered scan rates.

Additional simulations are carried out for the asymmetrical case, where the applied potential wave is not centred around the formal potential but slightly altered. As revealed by the data presented in the Supporting Materials S1 to S3, we herein observe analogous voltammetric behaviour: The heights of the first peak match the Randles-Ševčík equation for slow and fast scan rates and asymptotically approach different ultimate peak heights. We further observe that the peak-to-peak separation does not change with the scan number and unlike the peak heights is not altered during the experiment.

4.2 Irreversible electrode kinetics

Irreversible electrode kinetics were investigated for an electrochemical rate constant K_0 of 10^{-7}while all other parameters remain unchanged with respect to the simulations presented in Section 4.1. In contrast to the

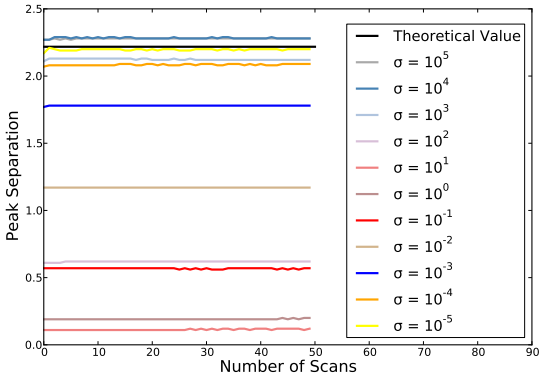

Figure 5: Peak-to-peak separation ΔE_{pp} in reversible symmetrical voltammograms for various scan rates as a function of the scan number. The indicated theoretical value depicts the result obtained from Equation (3).

reversible case there are however less analytical results with which to compare our simulations. The irreversible Randles-Ševčík equation as shown in Equation 2 however nonetheless provides a reference value for the height of the first peak.

Figure 6 presents data simulated for irreversible symmetric voltammograms at different scan rates. The data corresponding to the fast scan rate herein reveals that the first peak matches the theoretical prediction in terms of its height and the following scan asymptotically approach an 'ultimate voltammogram' featuring equal peak heights. In the intermediate case of a scan rate $\sigma = 1$, we find again that the peak heights are unaffected by the scan number as thin-layer diffusion dominates. For illustration we additionally show data for a scan rate close to the thin-layer limit were both, the current contribution of the thin-layer diffusion and diffusion from the bulk, can be seen in the voltammogram and peak splitting along the lines of Henstridge *et al.*[21] is observed. In short, this peak splitting is an immediate consequence of the interplay between mass transport phenomena and electrode kinetics. As previously elaborated, the observed voltammetric wave comprises components arising from thin layer diffusion within the pore as well as from material that diffusively reaches the electrode from the space above it. While in the reversible case the peak positions are independent of the scan rate and remain constant at 0 V and ± 28.5 mV for the two peaks, respectively, in the case of irreversible kinetics peak positions (and -currents) vary differently with the scan rate which results in the peak splitting observed at the two intermediate scan rates. In addition, even though at slow scan rates the peak splitting cannot be directly observed in the voltammogram, the effect underpinning such splittings remain and reduce the overall peak height, and hence, our data do not fit the theoretical results at the Randles-Ševčík limit.

The findings are further reflected in Figure 7, which illustrates the height of the positive peak as a function of the scan number and reveals that at fast and slow scan rate the 'ultimate voltammogram ' is asymptotically approached while in the intermediate regime the voltammogram is hardly affected by the scan number. In line with analytical theory, it can further be seen that the peak heights scale with the square root of the scan rates for the slow and fast scan rate regimes, respectively, and linearly if thin-layer diffusion dominates.

Figure 8 show the peak-to-peak separations observed in all irreversible symmetrical data as a function of the scan number, showing that ΔE_{pp} is independent of the repetition of the applied potential wave. Data that was recorded through multiple-cycle voltammetry can hence be directly compared with corresponding data obtained from conventional cyclic voltammetry if only peak-to-peak separations are considered.

As for the reversible case, additional irreversible simulations are carried out for a asymmetrical potential wave, where the voltammogram is not centred around the formal potential. As illustrated in the Supporting Materials S4 to S6, we again observe very similar voltammetric behaviour: The peak heights at slow and

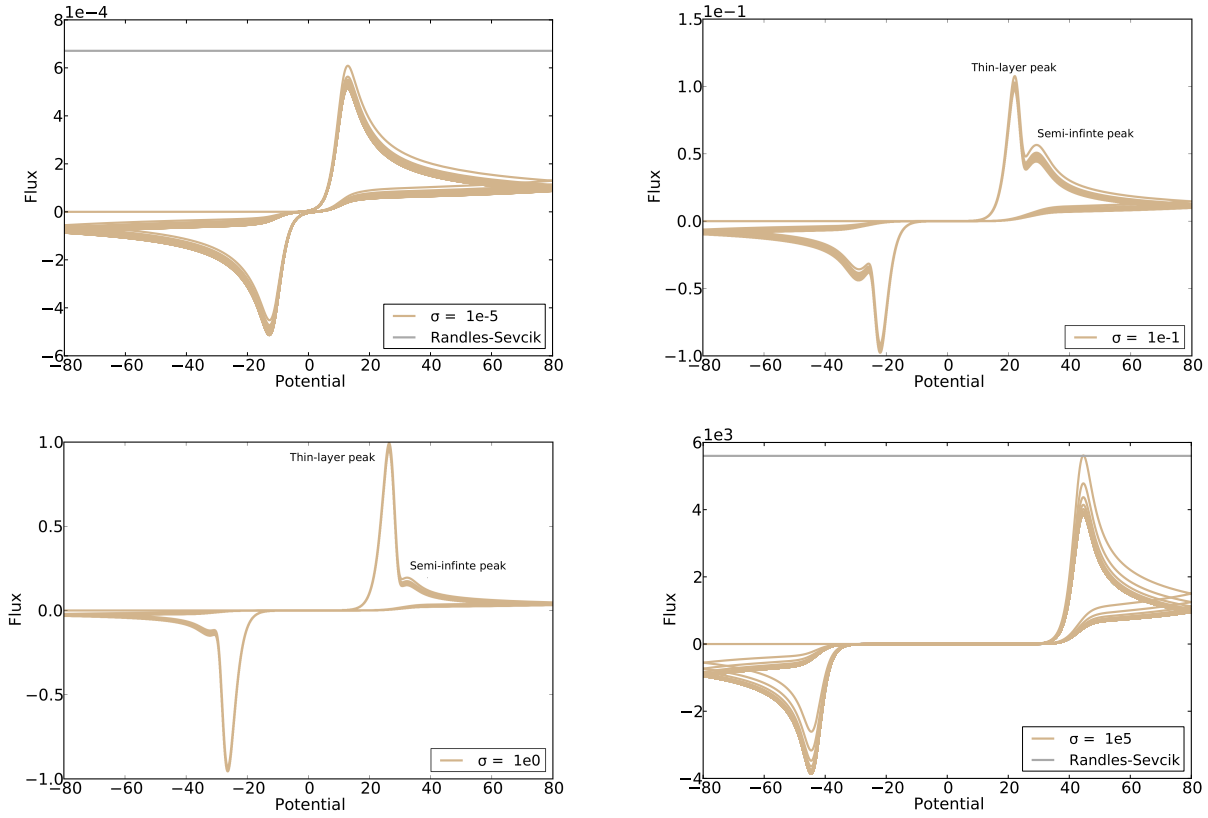

Figure 6: Irreversible symmetrical voltammograms modelled for scan rates of $\sigma = 10^{-5}$, 0.1, 1, and 10^5. For slow and fast scan rates it is plotted alongside the irreversible Randles-Ševčík equation (2) subject to the corresponding surface area, which is a) πr_{max}^2 and d) the surface area of the electrode. It is however noted that for the slowest considered scan rate, the theoretical peak height is solely plotted for illustrative reasons as the electrode kinetics are not fully reversible, the overall current is affected by peak splitting, and the peak height hence does not match the value it would reach in a one-dimensional system.

fast scan rates asymptotically approach different ultimate peak heights while peak heights in the thin-layer regime are unaffected by the scan number. As in all our simulations, we further observe that the peak-to-peak separation does not change with the scan number.

5 Conclusions

The presented work addresses the topic of multiple scan voltammetry at porous electrodes for the cases of reversible and irreversible electrode kinetics. Our results reveal that in the case of porous electrodes and if peak heights are considered, the common practise of running multiple scans until the voltammogram reaches a perceived ultimate state (or "waiting for it to stabilise") may lead to results that cannot be understood through classical theory such as Randles-Ševčík equation but can only be analysed considering the entire history of the system. We however identify two exceptions: If only the peak-to-peak separation is of interest or if the mass transport is dominated by thin-layer diffusion, results are independent of the repetition number. It is herein noted that our findings exclusively describe heterogeneous reactions featuring a 1:1 stoichiometry and fully reversible or -irreversible electrode kinetics in the absence of associated homogeneous reactions. As different processes may exhibit a different voltammetry, the presented results can be used as a reference for comparison with experimental multi-cycle data to indicate whether an anticipated mechanism may be prevalent. Quantities

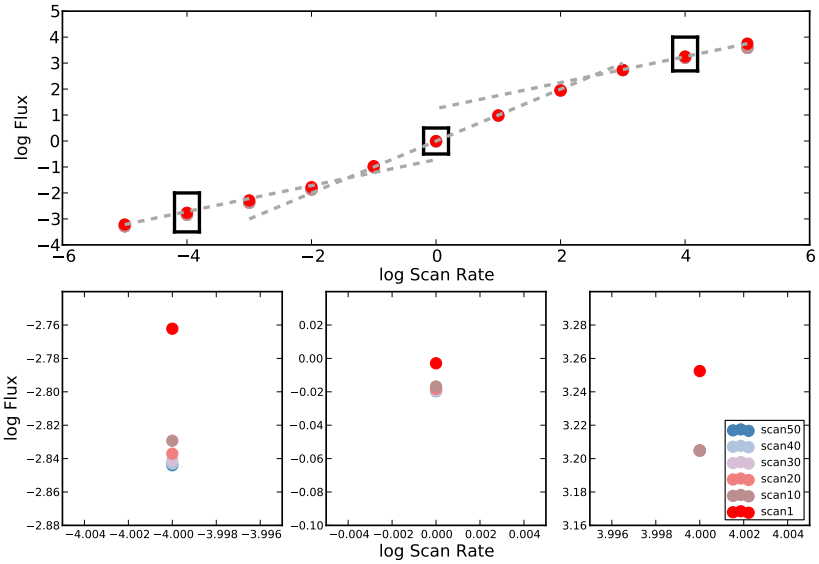

Figure 7: Maximum currents observed in irreversible symmetrical voltammograms at different scan repetitions and for various scan rates. Please compare Figure 4 for further details.

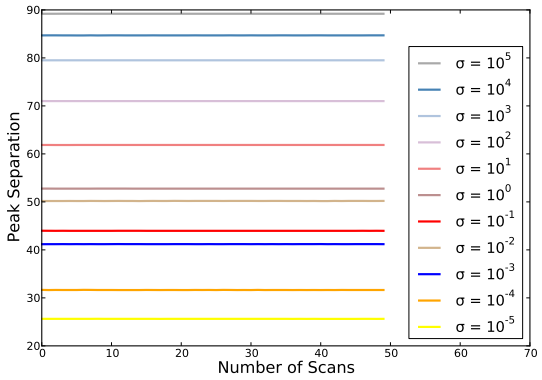

Figure 8: Peak-to-peak separation ΔE_{pp} in irreversible symmetrical voltammograms for various scan rates as a function of the scan number. Please note that in case of peak splitting the highest peak is considered in the analysis.

such as peak heights, peak-to-peak separations, and peak positions that are all provided in this work will be of help in this context.

Acknowledgements

The research leading to these results has received partial funding from the European Research Council under the European Union's Seventh Framework Programme (FP/2007-2013) / ERC Grand Agreement n. [320403].

References

[1] R. S. Nicholson and I. Shain. Theory of stationary electrode polarography. single scan and cyclic methods applied to reversible, irreversible, and kinetic systems. *Analytical Chemistry*, 36(4):706–723, 1964.

[2] R. S. Nicholson. Theory and application of cyclic voltammetry for measurement of electrode reaction kinetics. *Analytical Chemistry*, 37(11):1351–1355, 1965.

[3] A. J. Bard and L. R. Faulkner. *Electrochemical Methods: Fundamentals and Applications, 2nd Edition*. Wiley, 2001.

[4] R. G. Compton and C. E. Banks. *Understanding Voltammetry, 2nd Edition*. Imperial College Press, 2011.

[5] R. Guidelli, R. G. Compton, J. M. Feliu, E. Gileadi, J. Lipkowski, W. Schmickler, and S. Trasatti. Defining the transfer coefficient in electrochemistry: An assessment (IUPAC technical report). *Pure and Applied Chemistry*, 86(2):245–258, 2014.

[6] R. Guidelli, R. G. Compton, J. M. Feliu, E. Gileadi, J. Lipkowski, W. Schmickler, and S. Trasatti. Definition of the transfer coefficient in electrochemistry (IUPAC recommendations 2014). *Pure and Applied Chemistry*, 86(2):259–262, 2014.

[7] R. G. Compton, E. Laborda, and K. R. Ward. *Understanding voltammetry: Simulation of electrode processes*. Imperial College Press, 2013.

[8] K. B. Oldham. Ultimate cyclic voltammetry: An analytical examination of the reversible case. *Journal of Solid State Electrochemistry*, 17(11):2749–2756, 2013.

[9] K. B. Oldham. Multi-scan reversible cyclic voltammetry: Is the ultimate condition approached and, if so, how fast? *Journal of Solid State Electrochemistry*, 17(11):2757–2769, 2013.

[10] S. Sharma and B. G. Pollet. Support materials for PEMFC and DMFC electrocatalysts? a review. *Journal of Power Sources*, 208:96–119, 2012.

[11] H. Naatz, S. Lin, R. Li, W. Jiang, Z. Ji, C. H. Chang, J. Köser, J. Thöming, T. Xia, A. E. Nel, L. Mädler, and S. Pokhrel. Safe-by-design CuO nanoparticles via fe-doping, cu–o bond length variation, and biological assessment in cells and zebrafish embryos. *ACS Nano*, 11(1):501–515, 2017.

[12] Z. Ban, E. Kätelhön, and R.G. Compton. Voltammetry of porous layers: Staircase vs analog voltammetry. *Journal of Electroanalytical Chemistry*, 776:25–33, 2016.

[13] M. J. Sims, N. V. Rees, E. J .F. Dickinson, and R. G. Compton. Effects of thin-layer diffusion in the electrochemical detection of nicotine on basal plane pyrolytic graphite (BPPG) electrodes modified with layers of multi-walled carbon nanotubes (MWCNT-BPPG). *Sensors and Actuators B: Chemical*, 144(1):153–158, 2010.

[14] B. R. Scharifker. Diffusion to ensembles of microelectrodes. *Journal of Electroanalytical Chemistry and Interfacial Electrochemistry*, 240(1-2):61–76, 1988.

[15] T. J. Davies, C. E. Banks, and R. G. Compton. Voltammetry at spatially heterogeneous electrodes. *Journal of Solid State Electrochemistry*, 9(12):797–808, 2005.

[16] N. Godino, X. Borrisé, F. X. Muñoz, F. Javier del Campo, and R.G. Compton. Mass transport to nanoelectrode arrays and limitations of the diffusion domain approach: Theory and experiment. *The Journal of Physical Chemistry C*, 113(25):11119–11125, 2009.

[17] O. Sliusarenko, A. Oleinick, I. Svir, and C. Amatore. Validating a central approximation in theories of regular electrode electrochemical arrays of various common geometries. *Electroanalysis*, 27(4):980–991, 2015.

[18] B. A. Brookes, T. J. Davies, A. C. Fisher, R. G. Evans, S. J. Wilkins, K. Yunus, J. D. Wadhawan, and R. G. Compton. Computational and experimental study of the cyclic voltammetry response of partially blocked electrodes. part 1. nonoverlapping, uniformly distributed blocking systems. *The Journal of Physical Chemistry B*, 107(7):1616–1627, 2003.

[19] E. J. F. Dickinson, J. G. Limon-Petersen, N. V. Rees, and R. G. Compton. How much supporting electrolyte is required to make a cyclic voltammetry experiment quantitatively "diffusional"? a theoretical and experimental investigation. *The Journal of Physical Chemistry C*, 113(25):11157–11171, 2009.

[20] E. Kätelhön and R. G. Compton. Testing and validating electroanalytical simulations. *The Analyst*, 140(8):2592–2598, 2015.

[21] M. C. Henstridge, E. J. F. Dickinson, and R. G. Compton. Mass transport to and within porous electrodes. linear sweep voltammetry and the effects of pore size: The prediction of double peaks for a single electrode process. *Russian Journal of Electrochemistry*, 48(6):629–635, 2012.